ELSEVIER

Journal of Chromatography A, 770 (1997) 39–50

JOURNAL OF CHROMATOGRAPHY A

Continuous chromatographic separation process: simulated moving bed allowing simultaneous withdrawal of three fractions

A. Navarro, H. Caruel, L. Rigal*, P. Phemius

Laboratoire de Chimie Agro-Industrielle, INPT, U.A. INRA 31A1010, Ecole Nationale Superieure de Chimie de Toulouse, 118 Route de Narbonne, 31077 Toulouse Cedex, France

Abstract

Continuous counter-current chromatographic separation has been carried out in a simulated moving bed system (SMB). We have worked with a SMB pilot plant (8 columns, 4.4 litres of resin each) which allows the continuous withdrawal of two different fractions. A mixture of glucose–fructose has been separated. To calculate the concentration profile within the separator an axial dispersed plug flow model and an equilibrium stage model have been employed; software has been created to simulate the behaviour of the separator. The necessary parameters of the model: the adsorption equilibrium constant, the height equivalent to a theoretical plate and the bed voidage, have been acquired experimentally from elution chromatography measurements. The results calculated by simulation give a good representation of the experimental concentration profiles; other separations like xylitol–arabitol have been simulated. The influence of some factors like desorbent flow-rate, feed flow-rate and the bed voidage have been studied using the software. Once the system has worked in a two withdrawal way, an extension of the pilot plant has been constructed so as to obtain a third one. The necessary parameters of the three withdrawal model will be studied.

Keywords: Simulated moving bed chromatography; Continuous separation processes; Preparative chromatography; Carbohydrates

1. Introduction

The implementation of high-performance separation units constitutes a key stage in industrial development. Several chromatographic separation processes have been developed in the last years, proving this a technique of interest at an industrial scale [1]. Although batch chromatography is a relatively simple process offering operating flexibility, it suffers from a lot of difficulties like requirement of a large difference in the adsorptive selectivity of components and ineffectively use of adsorbent bed, among others [2]. In order to avoid all these disadvantages, continuous counter-current methods have been developed where mass transfer is maximized, thus a more efficient usage of the adsorbent is presented, requiring only a partial separation of components [3]. However such processes have the difficulties involved in circulating a solid adsorbent. Liquid chromatography in simulated moving bed (SMB) mode allows us to overcome these difficulties [4]. The first large-scale installations of this type were developed either by one compartment column or by several columns in series exemplified respectively by U.O.P. process [5] and Roquette Frères and Amalgamated sugar processes [6,7]. Although processes based on this concept have been developed for a number of commercially important separations of both aqueous and hydrocarbon systems in sugar and petrochemical industries, respectively [8,9], only limited informa-

*Corresponding author.

PII S0021-9673(96)01073-4

tion of a simulated moving bed with three outputs has been published [10]. The problem of modelling a simulated counter-current adsorption separation process has attracted a lot of attention recently. Ching and coworkers [11–15] have studied the theoretical and experimental behaviour of several binary mixtures in a SMB unit, using 12 columns of 100 cm×5.5 or 5.1 cm I.D. each. They have worked with both an equilibrium stage model and a dispersed plug flow model under linear and non-linear systems. They have made also a comparative study of flow schemes in SMB [16]. In a work by Ernst et al. [3,17] a theoretical analysis of a SMB process using a staged model has been carried out. They have investigated the effects of the backmixing factor. Design of SMB, paying attention in particular, to linear and non linear adsorption isotherms of binary mixtures has been made by Hashimoto et al. [18,19]. Lately Charton et al. [8] have presented a complete design of SMB using the equilibrium stage model. They focus on the separation of enantiomers mixture using 12 columns of 26 mm I.D.

The objective of this paper is to present a SMB pilot plant allowing binary mixture separation and its further modification providing ternary mixture separation as well. The implementation of a decision-helping tool has been developed to anticipate the behaviour of binary mixtures in the separator. It is based on a simple automated calculation software from two models presented in the literature. The decision-helping tool allows: (a) definition of the base operating conditions providing the theoretically expected fractions close to experimentally collected fractions, (b) study of the influence of the parameters and (c) predimension of an installation to a given production. Its modification enabling the anticipation of ternary mixture behaviour in the separator is also presented.

2. Experimental

The experimental system that we have installed in our laboratory is sketched in Fig. 1. The separator consists of eight identical glass jacketed columns, 150 cm×6.1 cm I.D. each, thermostated at 50°C by fluid circulation in the jacket, packed with Duolite cation-exchange resin in calcium form by the sedi-

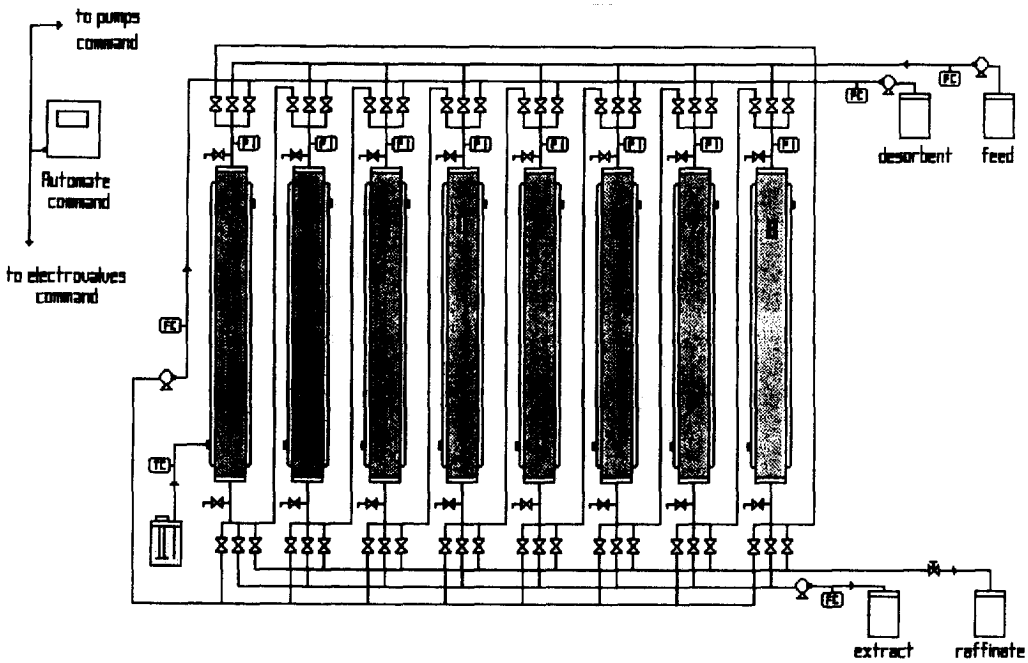

Fig. 1. Simulated moving bed pilot plant allowing binary mixture separation.

mentation method. The columns, linked in series, are connected through electrically controlled valves which allow feed to be introduced, product to be withdrawn or transfer of liquid to the next column. They are commanded by a programmable automat. Feed, extract, recirculation and desorbent flow-rates were controlled by rotary pumps. One of the outlet flow-rates is controlled manually. To determine the liquid phase concentration profiles within the separator, samples were withdrawn at regular intervals, each switch time from sample points located at the bottom of each column and analysed by HPLC. The quantity of liquid withdrawn in the samples was small compared with the total flow and the velocity can therefore be considered as essentially constant through the separator.

In simulated moving bed processes the adsorbent remains fixed in the separator advancing the concentration profile in the mobile phase flow direction through the separator. Once the concentration profile moves through one column it is necessary to advance inlets and outlets in the same way, in order to maintain their relative positions compared with it. The adsorbent bed counter current displacement will be simulated like that. The inlets and outlets will stand fixed as long as the concentration profile moves forward one column length again. This fixed time interval will be then called the switch time. At every switch time the inlets and outlets will be moved forward one column length in the direction of the fluid flow. In any counter-current mass transfer process the key parameter which governs the steady state concentration profile is the flow ratio:

$$\gamma = \frac{KS}{L} = \left(\frac{1-\varepsilon}{\varepsilon}\right)\left(\frac{u}{v}\right)K = \frac{KF_A}{F_{D,G}} \qquad (1)$$

Thus in order to achieve the fructose–glucose separation it is necessary to ensure the next flow constraints:

$$\left.\begin{array}{lll} \text{zone} & \text{I} & \gamma_F < 1, \gamma_G < 1 \\ & \text{II} & \gamma_F > 1, \gamma_G < 1 \\ & \text{III} & \gamma_F > 1, \gamma_G < 1 \\ & \text{IV} & \gamma_F > 1, \gamma_G > 1 \end{array}\right\} \qquad (2)$$

If: $\gamma < 1$, the component advances to the considering zone with the fluid flow; $\gamma > 1$, the component advances to the considering zone with the adsorbent.

2.1. Simulation

In order to generalise the usefulness of simulated counter-current chromatographic processes without carrying out all the corresponding experiments, we have used two equivalent counter-current models to simulate the behaviour of the separator. These two models need to acquire some chromatographic magnitudes from elution chromatography. From these parameters it will be possible to draw the chromatographic profiles in liquid and solid-phase if necessary, into the separator. The first model, model I, is an axial dispersed plug flow model worked by Ruthven and Ching [4]. Fig. 2 is a schematic diagram of such a model illustrating a system working in simulated moving bed mode. One can assume plug flow of the solid-phase with an equivalent velocity u, and axial dispersed plug flow for the fluid phase with an equivalent counter-current velocity v. The basic differential mass balance equation describing the system dynamics is then:

$$D_L\frac{\partial^2 c}{\partial z^2} - v\frac{\partial c}{\partial z} + \left(\frac{1-\varepsilon}{\varepsilon}\right)u\frac{\partial q}{\partial z} = \frac{\partial c}{\partial t} + \left(\frac{1-\varepsilon}{\varepsilon}\right)\frac{\partial q}{\partial t} \qquad (3)$$

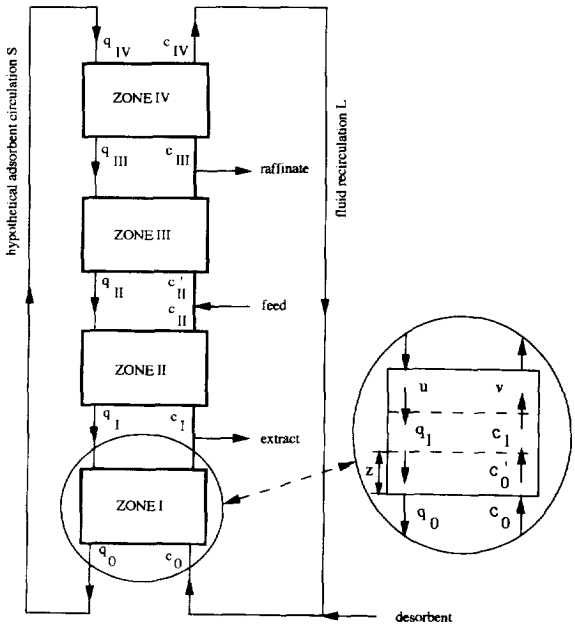

Fig. 2. Schematic diagram of model I showing two outputs (from Ref. [4]).

If we consider linear and uncoupled equilibrium isotherms and linear mass transfer rate, at steady state, Eq. (3) becomes:

$$D_L\frac{d^2c}{dz^2}-v\frac{dc}{dz}-\left(\frac{1-\varepsilon}{\varepsilon}\right)k(Kc-q)=0 \tag{4}$$

subject to the boundary conditions:

$$\left.\begin{array}{ll}\text{liquid inlet:} & z=0,\quad c_0=c'_0-\dfrac{D_L}{v}\left(\dfrac{dc}{dz}\right)_{z=0}\\ \text{liquid outlet:} & z=l,\quad \left(\dfrac{dc}{dz}\right)_{z=l}=0\end{array}\right\} \tag{5}$$

These equations may be expressed in dimensionless form and after some rearrangement using a mass balance over the bed, one obtains:

$$\left.\begin{array}{l}-\dfrac{d^2\phi}{dZ^2}+(\mathrm{Pe}+\mathrm{St})\dfrac{d\phi}{dZ}-\mathrm{Pe\,St}(1-\gamma)\phi+\mathrm{Pe\,St}\left(1-\dfrac{\gamma q_0}{Kc_0}\right)=0\\ \phi|_{Z=0}=1-Pe^{-1}\dfrac{d\phi}{dZ}\Big|_{z=0};\ \dfrac{d\phi}{dZ}\Big|_{Z=1}=0\end{array}\right\} \tag{6}$$

The relevant solution is:

$$\frac{\phi(1-1/\gamma)+1/\gamma-q_0/Kc_0}{1-q_0/Kc_0}=\frac{m_1e^{m_1+m_2Z}-m_2e^{m_2+m_1Z}}{m_1e^{m_1}(1-m_2/\mathrm{Pe})-m_2e^{m_2}(1-m_1/\mathrm{Pe})} \tag{7}$$

where $m_1(+)$ and $m_2(-)$ are given by:

$$m=\frac{1}{2}\left\{(\mathrm{Pe}+\mathrm{St})\pm[(\mathrm{Pe}+\mathrm{St})^2+4\mathrm{Pe\,St}(\gamma-1)]^{1/2}\right\} \tag{8}$$

The concentration ratio over a section of the bed is therefore given by:

$$\frac{\phi_L(1-1/\gamma)+1/\gamma-q_0/Kc_0}{1-q_0/Kc_0}=\frac{m_1-m_2}{m_1e^{-m_2}(1-m_2/\mathrm{Pe})-m_2e^{-m_1}(1-m_1/\mathrm{Pe})} \tag{9}$$

where $\phi_L=c_L/c_0$.

In the equilibrium limit where mass transfer resistance is negligible and dispersion of the profile is due entirely to axial mixing, $\mathrm{St}\to\infty$, $m_1\approx\mathrm{St}>>m_2=(1-\gamma)\mathrm{Pe}$, thus Eq. (9) reduces to $(1-\gamma)e^{\mathrm{Pe}(1-\gamma)}$ and the concentration profile over the bed becomes:

$$\frac{c_L}{c_0}=\frac{1}{\gamma-1}[(1-q_0/Kc_0)]e^{\mathrm{Pe}(1-\gamma)Z}+\gamma q_0/Kc_0-1 \tag{10}$$

where

$$\mathrm{Pe}=\frac{vl}{D_L}=2\frac{l}{H'}\left(\frac{v}{u+v}\right),\quad u=\frac{l}{\tau},\quad u+v=\frac{L'}{\varepsilon A}$$

A simple mass balance over the zone gives:

$$q_L=q_0+\frac{L}{S}(c_L-c_0) \tag{11}$$

For each of the four zones there is one expression of the form of Eq. (10) and one expression of the form of Eq. (11). Two additional equations are obtained from the mass balance for each component over the inlet points giving a set of ten equations relating the ten key concentrations.

The second model that we have used, model II, is a stage model worked by Ernst and Hsu [3]. The schematic diagram of such a model consisting of N stages and also divided in four zones is sketched in Fig. 3. At steady state, the total mass balance for the ith component around the jth stage in terms of the liquid phase concentrations with linear and uncoupled equilibrium isotherms yields:

$$\begin{aligned}&(F_{D,G}+f_{D,j}+K_{i,j}f_{A,j-1})c_{D,i,j-1}-(F_{D,G}+f_{D,j}+f_{D,j+1}\\&\quad+K_{i,j}F_{A,G}+K_{i,j}f_{A,j-1}+K_{i,j}f_{A,j})c_{D,i,j}\\&\quad+(f_{D,j+1}+K_{i,j}F_{A,G}+K_{i,j}f_{A,j})c_{D,i,j+1}=0\end{aligned} \tag{12}$$

If Eq. (12) is normalized with respect to the adsorbent flow-rate and the concentration of the component highest in the feed composition, one obtains:

$$\begin{aligned}&(\Phi_{D,G}+\beta_{D,j}+K_{i,j}\beta_{A,j-1})X_{D,i,j-1}-(\Phi_{D,G}+\beta_{D,j}\\&\quad+\beta_{D,j+1}+K_{i,j}\Phi_{A,G}+K_{i,j}\beta_{A,j-1}+K_{i,j}\beta_{A,j})X_{D,i,j}\\&\quad+(\beta_{D,j+1}+K_{i,j}\Phi_{A,G}+K_{i,j}\beta_{A,j})X_{D,i,j+1}=0\end{aligned} \tag{13}$$

Because there is no dispersive transfer of adsorbent from one stage to another ($f_{A,j}=0\to\beta_{A,j}=0$) and assuming each stage holds an equal amount of adsorbent ($F_{A,G}=F_A\to\Phi_{A,G}=1$) the mass balance

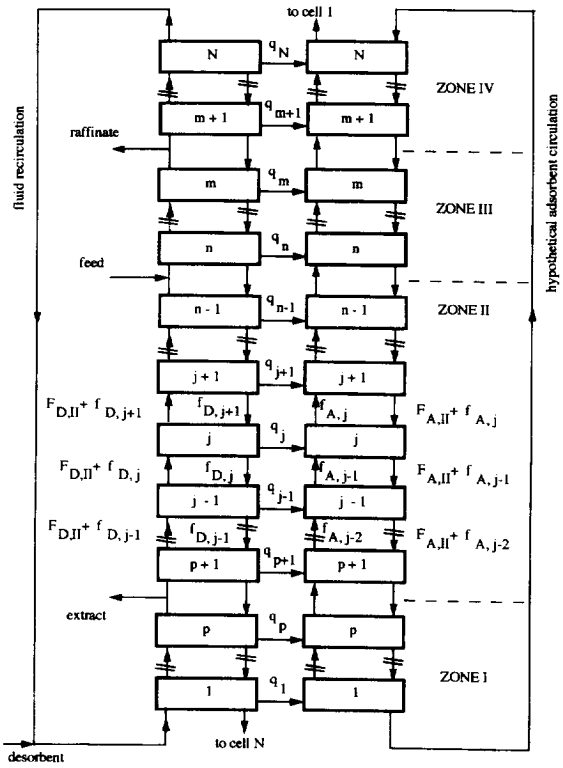

Fig. 3. Schematic diagram of model II showing two outputs (from Ref. [3]).

through the adsorbent bed becomes (assuming constant backmixing values, $\beta_{D,j} = \alpha = 0.67$):

For each jth stage where $j \neq 1,m,n,P,N$

$$A_j X_{D,i,j-1} + B_j X_{D,i,j} + C_j X_{D,i,j+1} = 0$$

where, $A_j = \Phi_{D,G} + \beta_{D,j}$; $B_j = -(\Phi_{D,G} + \beta_{D,j+1} + K_i)$; $C_j = \beta_{D,j+1} + K_i$.

For desorbent stage, $j = 1$:

$$A_1 X_{D,i,N} + B_1 X_{D,i,1} + C_1 X_{D,i,2} = -\Phi_D X_{D,I}$$

where, $A_1 = \Phi_{D,IV} + \beta_{D,1}$.

For extract stage, $j = p$:

$$A_p X_{D,i,p-1} + B_p X_{D,i,p} + C_p X_{D,i,p+1} = 0$$

where, $A_p = \Phi_{D,I} + \beta_{D,p}$; $B_p = -(\Phi_{D,II} + \beta_{D,p} + \beta_{D,p+1} + \Phi_E + K_i)$.

Feed stage, $j = n$:

$$A_n X_{D,i,n-1} + B_n X_{D,i,n} + C_n X_{D,i,n+1} = -\Phi_F X_{F,i}$$

where, $A_n = \Phi_{D,II} + \beta_{D,n}$.

Raffinate stage $j = m$:

$$A_m X_{D,i,m-1} + B_m X_{D,i,m} + C_m X_{D,i,m+1} = 0$$

where, $A_m = \Phi_{D,III} + \beta_{D,m}$; $B_m = -(\Phi_{D,IV} + \beta_{D,m} + \beta_{D,m+1} + \Phi_R + K_i)$.

Nth stage, $j = N$:

$$A_N X_{D,i,N-1} + B_N X_{D,i,N} + C_N X_{D,i,1} = 0$$

where, $B_N = -(\Phi_{D,IV} + \beta_{D,N} + \beta_{D,1} + K_i)$; $C_N = \beta_{D,1} + K_i$.

The resulting matrix obtained from Eq. (13) is presented in Table 1. The liquid phase concentration profiles may be directly obtained for individual components by solving this matrix.

Both of the models presented here need the following parameter acquisitions:

(a) The equilibrium isotherm (K). To calculate the equilibrium isotherm we have used the elution chromatography method. Several one column elution

Table 1
Resulting matrix for model II obtained from Eq. (13)

$$\begin{bmatrix} B_1 & C_1 & & & & & \\ A_2 & B_2 & C_2 & & & & \\ & \bullet & \bullet & \bullet & & & \\ & A_n & B_n & C_n & & & \\ & & \bullet & \bullet & \bullet & & \\ & & & \bullet & \bullet & \bullet & \\ & & & A_{N-1} & B_{N-1} & C_{N-1} & \\ & & & & A_N & B_N & \end{bmatrix} \begin{bmatrix} XD,i,1 \\ XD,i,2 \\ \bullet \\ XD,i,n \\ \bullet \\ \bullet \\ \bullet \\ XD,i,N \end{bmatrix} = \begin{bmatrix} -\Phi DXD,i \\ 0 \\ \bullet \\ -\Phi FXf,i \\ 0 \\ \bullet \\ \bullet \\ 0 \end{bmatrix}$$

chromatography separations were made varying both flow-rates and concentrations. The means and variances of the response peaks where calculated according to the following expressions [11]:

$$\left.\begin{aligned} \bar{t} &= \frac{\int_0^\infty ct\,dt}{\int_0^\infty c\,dt}, \quad \sigma^2 = \frac{\int_0^\infty c(t-\bar{t})^2 dt}{\int_0^\infty c\,dt} \end{aligned}\right\} \tag{14}$$

The mean retention time for a linear system is related to the equilibrium isotherm constant by:

$$\bar{t} = \frac{l}{\varepsilon v'}[\varepsilon + (1-\varepsilon)K] \tag{15}$$

Values of $\bar{t}$ were plotted against $(l/\varepsilon v')$ for both fructose and glucose. The resulting equilibrium isotherms derived from the slopes are shown in Table 2.

(b) The height equivalent to a theoretical plate (HETP). It has been estimated from elution chromatography measurements carried out under similar hydrodynamic conditions with one column in a fixed adsorbent bed. Assuming that the contribution to the HETP from mass transfer resistance must be small, we have:

$$H' = \frac{\Delta\sigma^2}{(\Delta\bar{t})^2 l} \tag{16}$$

Table 2 shows the values obtained by separations made at four different flow-rates covering the range of the counter-current experiments. Although the responses show little differences we consider the values to be constant for both fructose and glucose. Since the flow ratio is close to unity, the elution chromatography HETP is the half of counter-current HETP.

(c) Voidage of adsorbent bed (ε). The bed voidage within the column is defined as the ratio of interstitial liquid phase volume in the column to the total volume of the column. It was determined by measuring the liquid phase volume withdrawn from one column packed with adsorbent, obtaining a value of 0.38.

Table 2
Summary of elution chromatography measurements in fructose–glucose separation

Flow-rate (ml/min)	Fructose		Glucose	
	$\bar{t}$	H'	$\bar{t}$	H'
13.4	282	4.3	227	5.7
48	86	5.5	65	7.5
73.3	52	6.7	43	8.5

$K_F = 0.85$, $H'_F = 6$, $K_G = 0.52$, $H'_G = 8$.

3. Results

Once all of these parameters are defined, it is possible to obtain, by simulation, the chromatographic liquid phase profile within the separator for a fructose–glucose mixture of 390 g/l each with water as desorbent. The necessary parameters and the experimental conditions for both models are presented in Table 3. The configuration has been defined from the simulation, varying the repartition of the columns through the system within each zone. Comparison of theoretical and experimental profiles calculated from both models are represented in Figs. 4 and 5. The theoretical curves are predicted since they are derived from both the known inlet and outlet compositions and the necessary parameters without reference to the experimental profile. Although the values show some scatter, thus the agreement is not quantitatively exact, it is evident that the theoretical curves for both models provide a good representation of the experimental data. From model I, we can see that theoretical purities for both the extract and raffinate streams (88% and 87% respectively) are

Table 3
Summary of the necessary parameters and experimental conditions for both models with a mixture of fructose–glucose separation of 390 g/l each

Zone	Φ_D	L'	v	Pe_G	Pe_F	γ_G	γ_F
I	1.381	80	4.35	22.6	30.1	0.56	0.92
II	0.915	48	1.46	12.6	16.8	1.67	2.73
III	1.528	73	3.66	21	28	0.67	1.09
IV	0.950	50	1.62	13.5	18	1.51	2.46

$F_D = 30$, $F_E = 32$, $F_F = 25$, $F_R = 23$, $F_B = 50$, $S = 52.18$, $u = 2.88$, $\tau = 52$, $\varepsilon = 0.38$.
$K_G = 0.52$, $K_F = 0.85$, $H'_G = 8$, $H'_F = 6$, $\alpha = 0.67$, configuration: 3,1,2,2 (fructose = extract, glucose = raffinate).

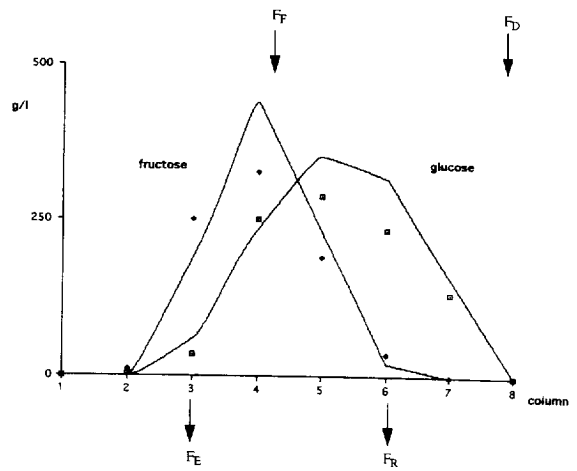

Fig. 4. Comparison of theoretical (points) and experimental (curves) profiles for fructose–glucose calculated by model I, from conditions described in Table 3.

very close to the experimental purities (76% and 94%, respectively). On the other hand, the differences between theoretical concentrations for both the extract and raffinate streams (250 g/l and 233 g/l, respectively) and experimental concentrations (190 g/l and 315 g/l, respectively) are slightly more important. Model II also gives a good representation of reality. For both the extract and raffinate streams the theoretical purities (83% and 88%, respectively)

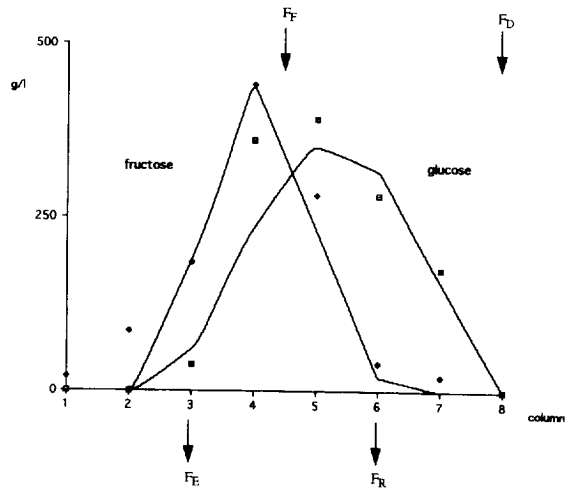

Fig. 5. Comparison of theoretical (points) and experimental (curves) profiles for fructose–glucose calculated by model II, from conditions described in Table 3.

and concentrations (185 g/l and 280g/l, respectively) are somewhat closer than experimental purities (76% and 94%, respectively) and concentrations (190 g/l and 315 g/l, respectively). The decision-helping tool presented in this paper, taking the scattering between theoretical and experimental data into account, does not allow a direct fit of the definitive operating conditions. Nevertheless it allows the SMB pilot plant to operate with conditions that are not so far away from the optimised searching conditions. We can see that the values obtained by simulation obtain a raffinate stream of 94% purity; the experimental optimisation should be made to the extract stream (76% of purity).

4. Discussion

In order to optimize the chromatographic separation, the influence of several factors were studied.

Equilibrium isotherm influence. A variation of K leads to a modification of the concentration profile whether by its position or by its height. A weak value of K means a poor retention by the adsorbent thus the response peak height is small. On the other hand when the values of K are higher than unity, the response peak height remains weak because of the difficulties to desorb the product from the adsorbent.

Bed voidage influence. Modification of ε leads to a change in the equilibrium isotherm because K has been determined by elution chromatographic measurements from Eq. (15). However we consider this parameter to be constant because we use only one kind of adsorbent at a time.

Adsorbent influence. The influence of the size of the support seems to be linked to that of the degree of cross-linking. With an important size of the support (350 μm particle size) the increase of the degree of cross-linking (>6% DVB) leads to an increase in the equilibrium isotherm value, thus a better separation. On the other hand with a weak resin size (225 μm particle size) the increase in the degree of cross-linking leads to a reduction of the equilibrium isotherm value because of the penetration difficulties of molecules to be separated inside the resin. These results can be compared with those of Caruel et al. [20] in the case of polyols mixture separation.

Influence of flow-rates. The flow-rates are linked one to another from the mass balance for each component over inlet and outlet points. The increase of the recirculation flow-rate leads to an increase in purities of extract and raffinate streams. Beyond 100 ml/min the purities do not change any more. On the other hand one can say that the variation of the desorbent flow-rate has an opposite behaviour over the extract and raffinate streams. The increase of the latter leads to a displacement of the less adsorbed component peak in the direction of fluid flow. Indeed, increase in both concentration of glucose at the raffinate withdrawal and purity of fructose at the extract withdrawal is obtained. Besides, the increase in desorbent flow-rate corresponds to a decreased concentration of fructose in the extract stream. The increase in feed flow-rate leads to a fast diminution in purity of the raffinate withdrawal and to an increase in purity of extract withdrawal. Moreover, the increase in extract flow-rate linked to the diminution in raffinate flow-rate leads to an increase of both the concentration and purity of the raffinate stream, whereas the concentration and purity of extract stream decrease proportionally. In this case, the sensibility of the extract stream purity is slightly less important with respect to raffinate stream purity.

4.1. Application to other separations

We then decided to apply model I to another binary mixture separation. We have simulated the separation of an arabitol–xylitol mixture of 100 g/l each. Table 4 shows the experimental conditions proposed as well as the necessary parameters to model I. They were obtained by elution chromatography measurements with water as desorbent and Purolite cation-exchange resin in calcium form. The decision-helping tool implementation has allowed us to establish the liquid phase concentration profiles of both the extract and raffinate products given in Fig. 6. This way, it has also been possible to define the conditions needed to carry out the separation aimed at the defined quality products. Thus the theoretical purities for both the extract and raffinate streams (87% and 96%, respectively) as well as the concentrations (85 g/l and 30 g/l, respectively) have been anticipated.

Table 4
Summary of the essential parameters and experimental conditions proposed to model I for arabitol–xylitol mixture of 100 g/l each

Zone	L'	v	Pe_A	Pe_X	γ_A	γ_X
I	95	5.43	31.74	31.74	0.8	1.22
II	80	4.07	28.26	28.26	1.07	1.63
III	100	5.87	32.61	32.61	0.74	1.14
IV	55	1.82	18.38	11.39	2.39	3.65

$F_D=40$, $F_E=15$, $F_F=20$, $F_R=45$, $F_B=55$, $S=56.7$, $u=3.13$, $\tau=48$.
$K_A=0.85$, $K_X=1.30$, $H'_A=6$, $H'_X=6$, $\varepsilon=0.38$, configuration: 3,1,2,2 (xylitol=extract, arabitol=raffinate).

Because of the empirical character of the dimensionless backmixing constant of model II, we have decided to use model I to consider ternary mixture separations. Adding a third withdrawal into the separator induces a fifth zone creation located at the top of the schematic diagram given in Fig. 7. Thus in order to achieve the mannitol–sorbitol–xylitol separation, the following flow constraints should be fulfilled:

$$\left.\begin{array}{lll} \text{zone} & \text{I} & \gamma_M<1,\ \gamma_S<1,\ \gamma_X<1 \\ & \text{II} & \gamma_M<1,\ \gamma_S>1,\ \gamma_X<1 \\ & \text{III} & \gamma_M<1,\ \gamma_S>1,\ \gamma_X>1 \\ & \text{IV} & \gamma_M<1,\ \gamma_S>1,\ \gamma_X>1 \\ & \text{V} & \gamma_M>1,\ \gamma_S>1,\ \gamma_X>1 \end{array}\right\} \quad (17)$$

The set of equations obtained by overall mass balance has been modified because of the additional zone. For each of the five zones there is one expression of the form of Eq. (10) and one expression of the form of Eq. (11). Two additional equations from the mass balance for each component over the feed points give a set of twelve equations relating to the twelve key concentrations. To solve this new set of equations, the simplified hypotheses that we have used in binary mixture separations remain the same. Fig. 8 shows the theoretical concentration profiles in liquid phase within the separator obtained by simulation of mannitol–sorbitol–xylitol mixture separation of 100 g/l each. Table 5 shows the experimental conditions proposed as well as the necessary parameters of the model. They were obtained with water as desorbent and Amberlite cation-exchange resin in calcium form, by elution chromatography measurements from Eqs. (15,16). The quality of extract one and two and

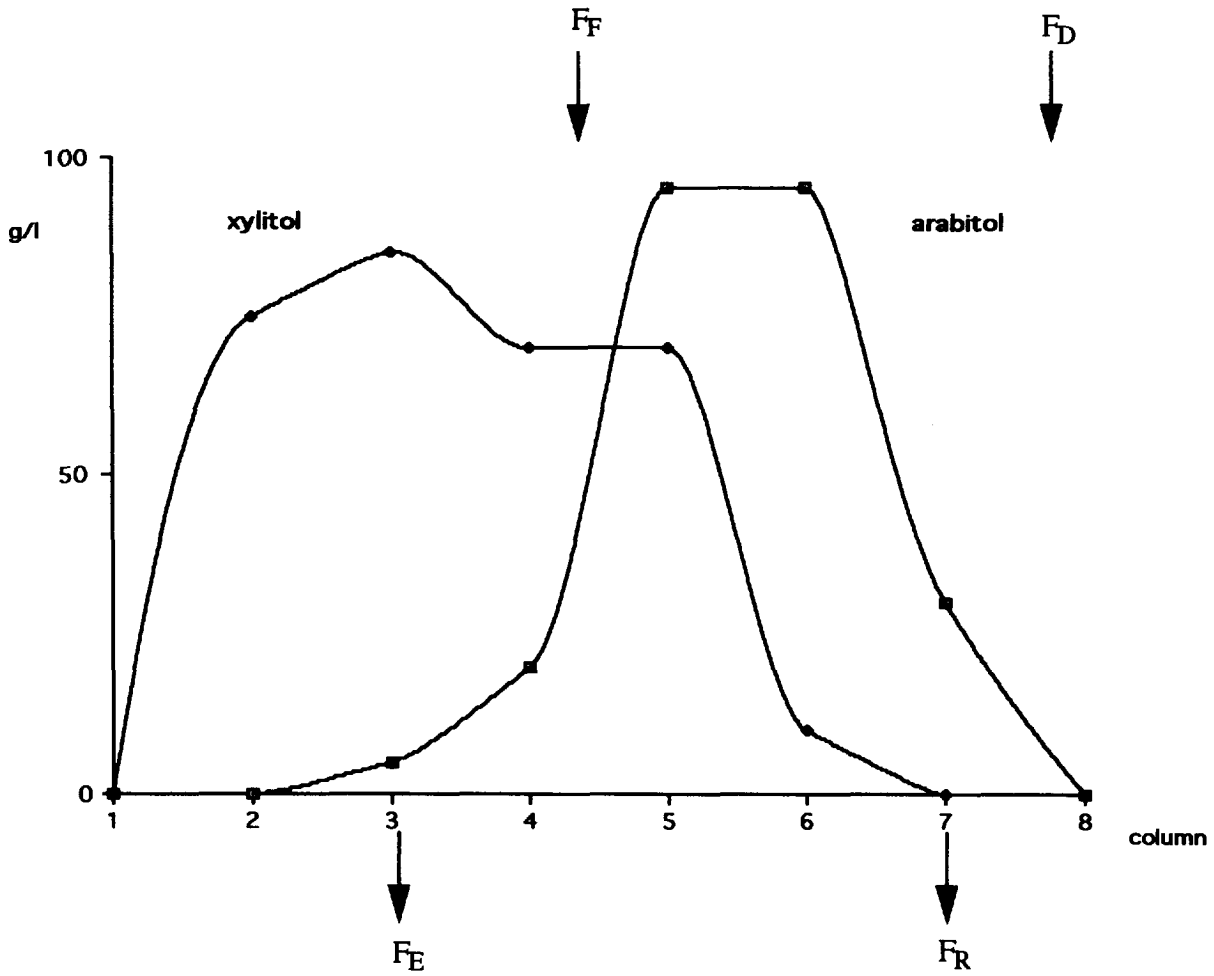

Fig. 6. Theoretical profiles for arabitol–xylitol calculated by model I, from conditions described in Table 4.

raffinate streams has been anticipated. Thus the theoretical purities for the extract, extract 2 and raffinate streams (58%, 38% and 94%, respectively) and the concentrations (59 g/l, 82 g/l and 31 g/l, respectively) have been predicted. This kind of separation largely justifies the use of a three withdrawal system. In the case of a two withdrawal system, the product having the intermediary equilibrium isotherm (xylitol) would not be withdrawn as a target product. It would go through the raffinate output decreasing the corresponding fractions purities. The withdrawn fraction of mannitol with high purity also justifies the implementation of the system presented in this paper. Actually, the purity of mannitol increases from 33% to 94%. Besides, it is well known that sorbitol–xylitol separation is difficult, as we have proved it in Ref. [21]. To improve this separation the support can be modified, but this is not the aim of this work. Although the conditions presented show some difficulties, the purity of sorbitol increases from 33% to 58%. The necessary modifications to the installation allowing a third outlet stream are presented in Fig. 9. In a general way, one additional rotary pump is necessary to achieve the withdrawal of the extract two stream. Also, one additional electrically controlled valve at the bottom of each column will be necessary to withdraw the third product and to switch its position.

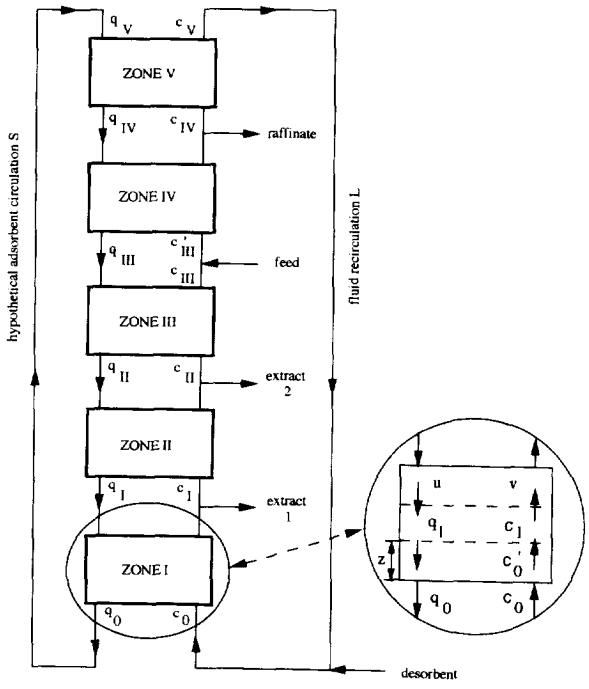

Fig. 7. Schematic diagram of the modified model showing three outputs.

5. Conclusion

One can say that both of the models worked in this paper have allowed us to establish a decision-helping tool in binary mixture separations. The close agreement between the results obtained by simulation and experimental values seems to be suitable for a first design of a SMB unit. It justifies the use of simpler steady state counter current models. Owing to these models we have observed the influence of several factors involved into the separation. Axial dispersed plug flow model modification for ternary mixtures has allowed us to produce a simulation of mannitol–sorbitol–xylitol mixture separation. This leads us to have the base operating conditions which allow us to consider further experimental separation.

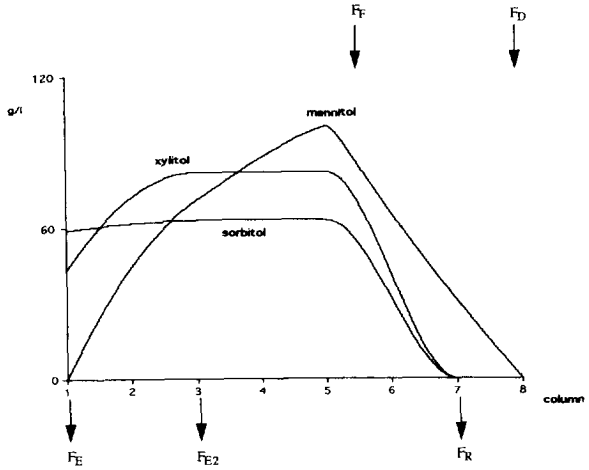

Fig. 8. Theoretical profiles for mannitol–sorbitol–xylitol calculated by model I modified from conditions described in Table 5.

Table 5
Summary of the necessary parameters and experimental conditions proposed for model I modified for mannitol–sorbitol–xylitol mixture 100 g/l each

Zone	L'	v	γ_M	γ_S	γ_X
I	130	7.9	0.7	1.1	0.9
II	110	6.1	0.9	1.3	1.2
III	90	4.3	1.3	1.8	1.6
IV	115	6.6	0.9	1.2	1.1
V	80	3.4	1.6	2.3	2.1

$F_D = 50$, $F_E = 20$, $F_{E2} = 20$, $F_F = 25$, $F_R = 35$, $F_B = 70$, $S = 52$, $u = 2.88$, $\tau = 52$.
$K_M = 1.19$, $K_S = 1.69$, $K_X = 1.5$, $H'_M = 7$, $H'_S = 5$, $H'_X = 5$, $\varepsilon = 0.38$, configuration: 1,2,2,2,1 (sorbitol = extract, xylitol = extract, mannitol = raffinate).

Acknowledgments

The authors thank Mexico's CONACYT for financial support and APPLEXION Society for contribution to this work.

Appendix 1

Symbols

A_j	matrix coefficient for stage j with respect to the variable for stage $j-1$
B_j	matrix coefficient for stage j with respect to the variable for stage j
C_j	matrix coefficient for stage j with respect to the variable for stage $j+1$
c	fluid phase concentration
c_0	fluid phase inlet concentration

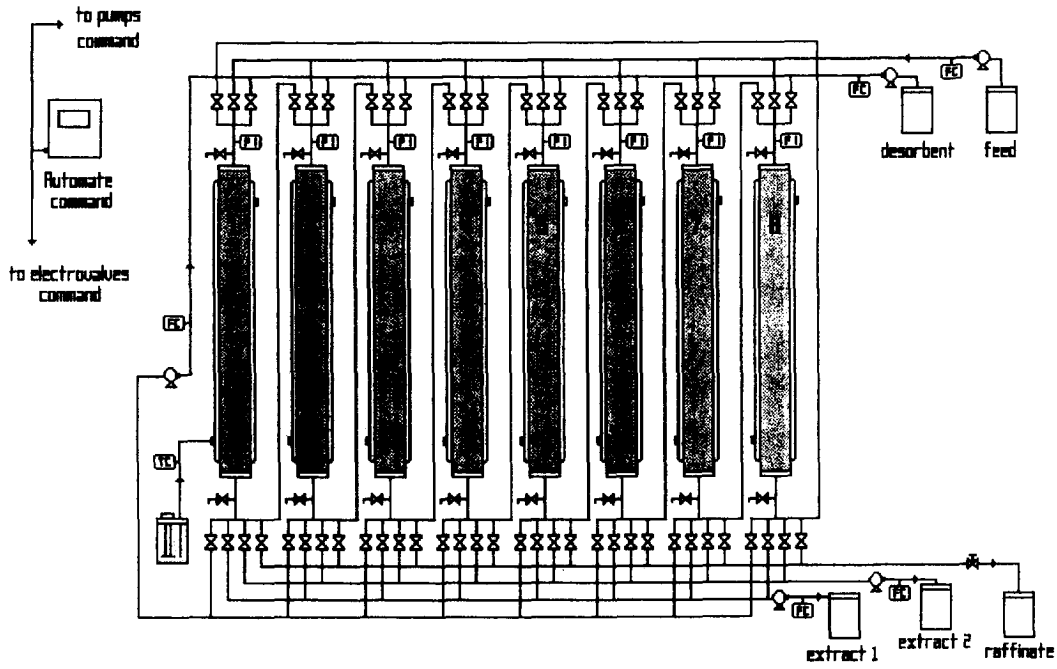

Fig. 9. Simulated moving bed pilot plant allowing ternary mixture separation.

c_0' fluid phase concentration just inside the bed

$c_{A,i,j}$ concentration of the ith component for the stage j in adsorbent phase, $(=K_{i,j}\, c_{D,i,j})$, g/l

$c_{D,i,j}$ concentration of the ith component for the stage j in liquid phase, g/l

$C_{F,i}$ concentration of the ith component in the feed, g/l

D_L axial dispersion coefficient $[=(H'/2)(u+v)]$, cm^2/min

F_A constant adsorbent flow-rate, ml/min

F_D desorbent flow-rate, ml/min

F_E extract flow-rate, ml/min

F_{E2} flow-rate of extract two, ml/min

F_F feed flow-rate, ml/min

F_R raffinate flow-rate, ml/min

F_B recirculation flow-rate, ml/min

$F_{D,G}$ constant liquid flow-rate for zone G, ml/min

$f_{D,j}$ backmixing liquid flow-rate for stage j, ml/min

$f_{A,j}$ backmixing flow-rate in adsorbent phase for stage j, ml/min

H HETP for counter current process, cm

H' HETP for chromatographic system, cm

H'_F HETP of fructose for chromatographic system, cm

H'_G HETP of glucose for chromatographic system, cm

k overall mass transfer rate coefficient, min^{-1}

K dimensionless adsorption equilibrium constant

K_A dimensionless adsorption equilibrium constant of arabitol

K_F dimensionless adsorption equilibrium constant of fructose

K_G dimensionless adsorption equilibrium constant of glucose

K_M dimensionless adsorption equilibrium constant of mannitol

K_S dimensionless adsorption equilibrium constant of sorbitol

K_X dimensionless adsorption equilibrium constant of xylitol

l length of individual column or zone, cm

L liquid flow-rate expressed on equivalent counter current basis $(=\varepsilon vA)$, ml/min

L' actual liquid flow-rate $[=\varepsilon A(u+v)]$, ml/min

Pe	Peclet number $[=vl/D_L=(2l/H')(v/u+v)]$
Pe_A	Peclet number of arabitol
Pe_F	Peclet number of fructose
Pe_G	Peclet number of glucose
Pe_X	Peclet number of xylitol
q	adsorbed phase concentration
$q_{i,j}$	net interphase flux of the ith component for stage j, g/l
S	solid flow-rate expressed on equivalent counter current basis $[=(1-\varepsilon)uA]$, ml/min
St	Stanton number $(=kl/u)$
t	time, min
$\bar{t}$	mean retention time, min
u	equivalent counter current solid velocity $(=l/\tau)$, cm/min
v	equivalent interstitial counter current liquid velocity, cm/min
v'	interstitial velocity of fluid, cm/min
$X_{A,i,j}$	dimensionless concentration of the ith component for stage j in the adsorbent phase $(=c_{A,i,j}/c_{F,i\ max})$
$X_{D,i,j}$	dimensionless concentration of the ith component for stage j in the mobile phase $(=c_{D,i,j}/c_{F,i\ max})$
z	axial distance, cm
Z	dimensionless axial distance $(=z/l)$

Greek letters

α	dimensionless backmixing constant
$\beta_{A,j}$	dimensionless volumetric backmixing flow-rate in the adsorbent phase $(=f_{A,j}/F_A=0)$
$\beta_{D,j}$	dimensionless volumetric backmixing flow-rate in the desorbent phase $(=f_{D,j}/F_A=\alpha)$
γ	flow ratio $(=KS/L=(1-\varepsilon/\varepsilon)(u/v)K)$
γ_A	flow ratio of arabitol
γ_F	flow ratio of fructose
γ_G	flow ratio of glucose
γ_M	flow ratio of mannitol
γ_S	flow ratio of sorbitol
γ_X	flow ratio of xylitol
ε	bed voidage
τ	switch time, min
σ	variance of the response peak
$\Phi_{A,G}$	dimensionless hypothetical adsorbent flow-rate $(=F_{A,G}/F_A=1)$
$\Phi_{D,G}$	dimensionless mobile phase flow-rate for zone G $(=F_{D,G}/F_A)$
Φ_D	dimensionless desorbent flow-rate $(=F_D/F_A)$
Φ_E	dimensionless extract flow-rate $(=F_E/F_A)$
Φ_F	dimensionless feed flow-rate $(=F_F/F_A)$
Φ_R	dimensionless raffinate flow-rate $(=F_R/F_A)$

References

[1] P. Phemius, Thèse de Docteur, Institut National Polytechnique, Toulouse, 1993.
[2] C.B. Ching and D.M. Ruthven, Can. J. Chem. Eng., 62 (1984) 398.
[3] U.P. Ernst and J.T. Hsu, Ind. Eng. Chem. Res., 28 (1989) 1211.
[4] D.M. Ruthven and C.B. Ching, J. Chromatogr. Sci., 61 (1993) 629.
[5] D.B. Broughton and C.G. Gerhold, US Pat., 2 985 589 (1961).
[6] F. Devos, D. Delobeau, J.J. Caboche, P. Lemay and M. Huchette, Fr. Pat., 7 910 563 (1979).
[7] K.W.R. Schoenrock, US Pat., 4 412 866 (IPN, W084/02854).
[8] F. Charton and R. Nicoud, J. Chromatogr. A, 702 (1995) 97.
[9] G. Hotier and B. Balannec, Rev. Inst. Pétrole, 46 (1991) 803.
[10] K.B. Kim, S. Kishihara and S. Fuji, Biosc. Biotech. Bioch., 56 (1992) 801.
[11] C.B. Ching and D.M. Ruthven, Chem. Eng. Sci., 40 (1985) 877.
[12] C.B. Ching, D.M. Ruthven and K. Hidajat, Chem. Eng. Sci., 40 (1985) 1411.
[13] C.B. Ching, C. Ho, K. Hidajat and D.M. Ruthven, Chem. Eng. Sci., 42 (1987) 2547.
[14] C.B. Ching, C. Ho and D.M. Ruthven, Chem. Eng. Sci., 43 (1988) 703.
[15] C.B. Ching, K.H. Chu, K. Hidajat and D.M. Ruthven, Chem. Eng. Sci., 48 (1993) 1343.
[16] C.B. Ching, K.H. Chu, K. Hidajat and M.S. Uddin, AIChE J., 38 (1992) 1744.
[17] U.P. Ernst and J.T. Hsu, Sep. Technol., 2 (1992) 198.
[18] K. Hashimoto, Y. Shirai, M. Morishita and S. Adachi, J. Chem. Eng. Jpn, 25 (1992) 453.
[19] K. Hashimoto, S. Adachi, Y. Shirai and M. Morishita, J. Chromatogr. Sci., 61 (1993) 273.
[20] H. Caruel, P. Phemius, L. Rigal and A. Gaset, J. Chromatogr., 594 (1992) 125.
[21] H. Caruel, L. Rigal and A. Gaset, J. Chromatogr., 558 (1991) 89.